J Low Temp Phys (2007) 149: 105–118
DOI 10.1007/s10909-007-9500-0

Structural and Physical Properties of Nd Substituted Bismuth Cuprates $Bi_{1.7}$ $Pb_{0.3-x}Nd_xSr_2Ca_3Cu_4O_{12+y}$

Berdan Özkurt · Ahmet Ekicibil · M. Ali Aksan · Bekir Özçelık · M. Eyüphan Yakıncı · Kerim Kiymaç

Received: 17 March 2007 / Revised: 18 May 2007 / Published online: 26 July 2007

Abstract BiPb-2234 bulk samples with nominal composition of the compound $Bi_{1.7}Pb_{0.3-x}Nd_xSr_2Ca_3Cu_4O_{12+y}$ (BSCCO) ($0.025 \leq x \leq 0.10$) have been prepared by the melt-quenching method. The effects of Nd substitution on the BSCCO system have been investigated by electrical resistance (R–T), scanning electron microscopy (SEM), X-ray diffraction (XRD) and magnetic hysteresis measurements. It has been the BSCCO (2212) low-T_c phase is formed for all the substitution levels, together with the BSCCO (2223) high-T_c phase. The results obtained suggest that with increasing Nd^{3+} doping for Pb^{2+} the (2223) phase existing in undoped BSCCO gradually transforms into the (2212) phase and hence all of the samples have a mixed phase formation. The R–T result of the samples show two-step resistance transition; first transition occurs at 100 K and second in an interval of 80–90 K, depending on the Nd concentration. We have found that the magnetization decreases with increasing temperature in agreement with the general characteristic of the high-T_c materials. The samples exhibit weak field dependence particularly after 2 T and changes on the magnetic hysteresis, M–H curve rather small compared to the conventional superconducting materials. The maximum critical current density, J_c, value was calculated to be 8.51×10^5 at 4.2 K and J_c decreases with increasing temperature and the substitution level.

Keywords High T_c superconductors · Microstructure · X-ray diffraction · Magnetization and critical current density

PACS 74.60 Ej · 74.62.Dh · 74.72.Hs · 74.25 Ha · 74.25-q · 74.25 Sv

B. Özkurt · A. Ekicibil (✉) · B. Özçelık · K. Kiymaç
Department of Physics, Faculty of Sciences and Letters, Çukurova University, 01330 Adana, Turkey
e-mail: ahmetcan@cu.edu.tr

M. Ali Aksan · M.E. Yakıncı
Department of Physics, Faculty of Sciences and Letters, İnönü University, 44069 Malatya, Turkey

1 Introduction

It is well known that the superconductivity is suppressed by the presence of magnetic ions in the conventional metallic superconductors. This phenomenon can be understood in terms of the pair-breaking mechanism. On the other hand, the existence of some magnetic rare-earth metallic superconductors has been explained by claiming that the superconductivity and the magnetism take place in different parts of the sample, with little interaction between the two. However, in the case of all high-T_c ceramic superconductors, the CuO_2 planes, which contain Cu^{2+} ions, enhance the superconductivity, instead of degrading [1]. As it is well known fact, that the fundamental properties of superconductors are zero resistivity and Meissner effect. In addition, the common feature of the new family high-T_c superconductor is their layered structure along the c-axis comprising the existence of CuO_2 planes. Now, it is widely accepted that pairs of holes doped in these planes are responsible for the high temperature superconductivity. Furthermore, it is generally believed that the $Bi_2Sr_2CaCu_2O_{8-x}$ high temperature superconductor has extremely large anisotropies between the a–b plane and c-axis direction, and very weak bulk pinning above and about 30 K.

One can conclude that in most cases, substitution of "native" ions by foreign ions leads to a transition from superconductivity to antiferromagnetism or vice versa. The real coexistive cases of the phenomena are rare [2] and controversial, mainly because of the question of homogeneity of the samples. However, it seems quite clear that whenever the substitution decreases the number of charge carriers (either holes or electrons), the superconductivity is suppressed.

Weak coupling between BiO–BiO layers in the BSCCO system enables the substitution of the different oxides for Bi^{3+} site. Some of the results have demonstrated that there is no significant increase in the T_c. But, important changes occur in the carrier concentration due to the different cation doping levels. Therefore, the electrical property of the system varies. Here, we should state that the preparation technique of a system is also very important. To this end preparing the BSCCO system by the glass-ceramic technique yields good density and minimum porosity, compared to the conventional solid state technique [3–5].

The formation of pure and textured (2223) phase is a critical issue in fabricating BSCCO superconductors. Since the reaction kinetics of the Bi-(2223) phase formation is slow, long periods of sintering at temperatures close to its decomposition temperature are required [6]. Many factors, including composition, phase assemblage of the precursor powder, lead content, grain alignment, intergrain connectivity, density of the core, sintering parameters and doped ions, significantly influence the heat treatment parameters and final physical properties of the samples [7]. T_c of superconducting copper-oxide based compounds depends on the density of mobile holes in the CuO_2 planes and thus on the average Cu valancy [8]. The replacement of Pb^{2+} or Bi^{3+} ions by Nd^{3+} and co-doping Tb^{3+} and Nd^{3+} ions leads to a decrease of the formal Cu valancy [9, 10], whereas, the substitution of Pb^{2+} in Bi^{3+} site increases Cu valancy [11]. As a result, thus T_c, decreases with increasing Nd content, whereas it increases with a small amount of Pb substitution. However, the value of T_c can further be increased either by quenching or by annealing under reduced pressures (vacuum

or nitrogen), because T_c shows a strong dependence on the preparation conditions [40, 41].

As stated previously it has now been well established that the superconducting properties of the copper oxide superconductors are related to the hole concentration. Tarascon et al. [12] studied various substitutions of rare earths R^{3+} for Ca^{2+} in the $Bi_4Sr_4Ca_{2-x}R_xCu_4O_y$ system ($x \geq 1.0$) and reported that for $x \geq 1.5$ the compounds became semiconducting. But, for low doping levels ($x \leq 0.5$), T_c was not much affected. No magnetic ordering was observed down to 1.5 K. They further found that the depression of T_c occured no matter if the dopant was magnetic or non-magnetic and that the superconducting properties were strongly affected by changes in the hole concentration induced by the amount of doping. Yamanaka et al. [13] investigated the changes in the electronic states in $Bi_2Sr_2Ca_{1-x}Nd_xCu_2O_y$ ($0 \leq x \leq 1$) by X-ray photoelectron spectroscopy. They specifically selected Nd because its ionic radius is close to that of Ca to make the lattice distortion small. Their studies indicated that the holes at both Cu and O sites decrease with increasing Nd concentration. Kishore et al. [14] showed that the Sm^{3+} and Gd^{3+} substitutions in $Bi_2Sr_2Ca_{1-x}Dy_xCu_2O_y$ were responsible for the magnetic properties in both the normal and superconducting states.

Nevertheless, there are few reports on the effects of rare earth ion substitutions in the BSCCO (2223) system. Kanai et al. [15] reported that the substitution of rare earth ions for Ca brings about a transition from the (2223) to the (2212) phase. Rateau et al. [16] reported that the substitution of Sm, Nd and Gd decreases the hole carrier concentration causing a degradation of the high-T_c phase. Simon et al. and Bornemann [17, 18] studied the effect of Gd substitution for Ca and found that the magnetic Gd^{3+} ion depressed the superconducting transition temperature.

As compared to most of the other rare earths, the magnetic moment of Nd^{3+} is much higher and thus one can expect its significant effects on the magnetic as well as the superconducting properties (such as flux pinning) of a compound when doped with it [19, 20]. In order to explore this expectation, in this work, we have studied the effects of Nd^{3+} substitution for Pb^{2+} in dilute concentrations of $Bi_{1.7}Pb_{0.3-x}Nd_xSr_2Ca_3Cu_4O_{12+y}$ ($x = 0.025, 0.050, 0.075, 0.1$) compounds. To find out those effects microstructural, electrical and, magnetic properties of compounds have been explored.

2 Experimental Details

The appropriate amounts of Bi_2O_3, PbO, Nd_2O_3 $SrCO_3$, CaO, and CuO fine powders in the stoichiometric ratios of $Bi_{1.7}Pb_{3-x}Nd_xSr_2Ca_3Cu_4O_{12+y}$ ($x = 0.025, 0.050, 0.075, 0.1$) were well mixed by milling and calcined at 750°C for 10 h in air. The calcined powders were placed in a platinum crucible and heated at 1150°C until the samples were completely melted. The melts were poured onto a pre-cooled copper plate and pressed quickly by another cooper plate to obtain approximately 1.5 to 2 mm thick plate like amorphous (glass) material. The glass materials then crushed and grained to obtain fine glass powders. The mixture re-grinded about one hour and the resulting powder was then pressed into pellets of 10 mm diameter by applying

a pressure of 4 tonnes/cm^2. Finally, the precursor materials produced were annealed at 850°C for 170 h in air to achieve crystallized material and superconductivity. The samples with x values of 0.025, 0.050, 0.075 and 0.10 are denoted as A, B, C and D, respectively.

X-ray powder diffraction analyses were performed by using Rigaku RadB powder diffractometer system with CuKα radiation and a constant scan rate between $2\theta = 3$–60°. The microstructural and compositional characterizations were carried out with LEO Evo-40 VPX scanning electron microscope (SEM) and Röntec energy dispersive X-ray spectroscopy (EDX). Resistivity and magnetization measurements under different magnetic fields were carried out using Cryogenic Q-3398 Vibrating Sample Magnetometer (VSM) system.

3 Result and Discussions

The results obtained for the samples A, B, C and D ($x = 0.025, 0.05, 0.075, 0.1$) are shown in Figs. 1a–d, respectively. The X-ray diffraction results show multiphase, BiPb-2212 and BiPb-2223, structure throughout the substitutional range. CuO was also detected as an impurity phase. The crystal symmetry of the samples were found to be tetragonal and calculated unit-cell parameters are given in Table 1.

As seen in Table 1, with increasing x, a monotonic decreasing of the c-parameter with simultaneous increasing of the a-parameter were observed and this correlates with the decreasing hole concentration in the CuO_2 plane, as suggested by Satyavathi et al. and Zandbergen et al. [21, 22]. It was considered that even small amount

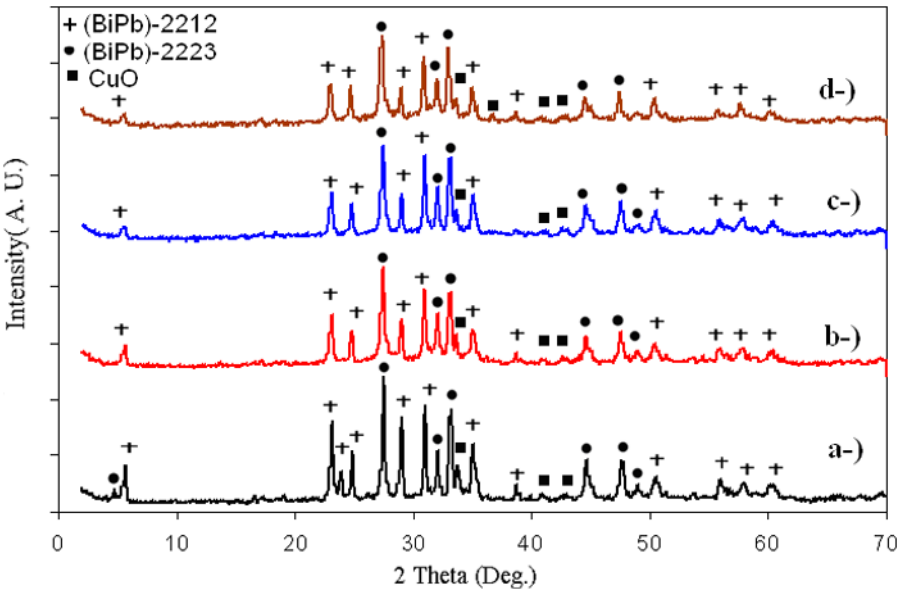

Fig. 1 (Color on-line) XRD result of (**a**) $x = 0.025$, (**b**) $x = 0.05$, (**c**) $x = 0.075$ and (**d**) $x = 0.1$ samples

Table 1 Unit cell parameters of the samples

Sample name	a, Å	b, Å	c, Å
A	5.3998	5.3998	30.8839
B	5.4004	5.4004	30.8101
C	5.4077	5.4077	30.7594
D	5.4103	5.4103	30.7063

of Nd^{3+} occupation of main matrix, which is believed that Nd^{3+} goes into the bismuth oxide layers in the main matrix and increases the oxygen content. This should produce a distortion on the lattice structure, that makes an increase on the a-axis parameter and consequently a decrease on the c-axis parameter. A slight increase in cell volume was observed, in contrast to the Sm substituted samples where it remained almost the same up to $x = 0, 1$ and increased thereafter [23, 24]. With increasing Nd concentration the oxygen content increases and this may be a reason of the decrease in the c-axis. We believed that Nd atoms may diffuse into the interstitial sites in the material rather than occupation of the Bi sites. If the valance states of the Bi and Nd are supposed to be unchanged in the material (Bi^{3+} and Nd^{3+}), since the ionic radius of Nd (1.85 A) is different from Bi^{3+} (0.96 A), distorted band structure and thus a change on the unit cell parameters. Similar results were previously obtained by other research groups for BSCCO material [25–27]. We have found no impurity phase other than CuO, which possibly comes trough the cooper plates during quenching process and not dissolved completely in the matrix during heat treatment cycles.

The SEM photographs for A, B, C and D samples are shown in Figs. 2a–d, respectively. It is clearly seen that formations of the surface morphology of the samples with different Nd concentration are almost similar. Randomly oriented, closely packed and dense flake-like grains with approximately 2–10 μm in size were formed all over the substitutional range which is the typical glass-ceramic BSCCO structure.

The microqualitative analyses of the samples have been done on the polished surfaces of the samples, and show Figs. 3a–d. All of the samples have shown three different phase formations but in general similar crystallization and hence almost the same compositions were observed for all substitution levels. According to EDX analysis, we have found only Ca and Sr contaminated CuO as an impurity phase and no Nd contaminated impurities were obtained. The main phases were found to be BiPb-2212 and BiPb-2223 superconducting phases for all the samples. This is in consistent with the XRD results of the samples. The polished surface of the samples also showed highly dense and strongly connected grains, which is the general characteristics of glass-ceramic materials, as expected [42–45].

The temperature dependence of the resistance (R–T) measurement results between 0 and 6 T are shown in Figs. 4a–d. Zero field cooling (ZFC) procedure was used during all measurements. It was obtained that all the resistances measured at zero magnetic field, decrease almost linearly with temperature in the normal state, and show two onset transition temperatures. This behavior points out that the samples have two phases, namely BiPb-2223 and BiPb-2212, as we have indicated previously in the XRD and SEM investigations. The Bi-2223 phase smears out with increasing magnetic field and, hence almost the BiPb-2212 phase remains for all the samples [46].

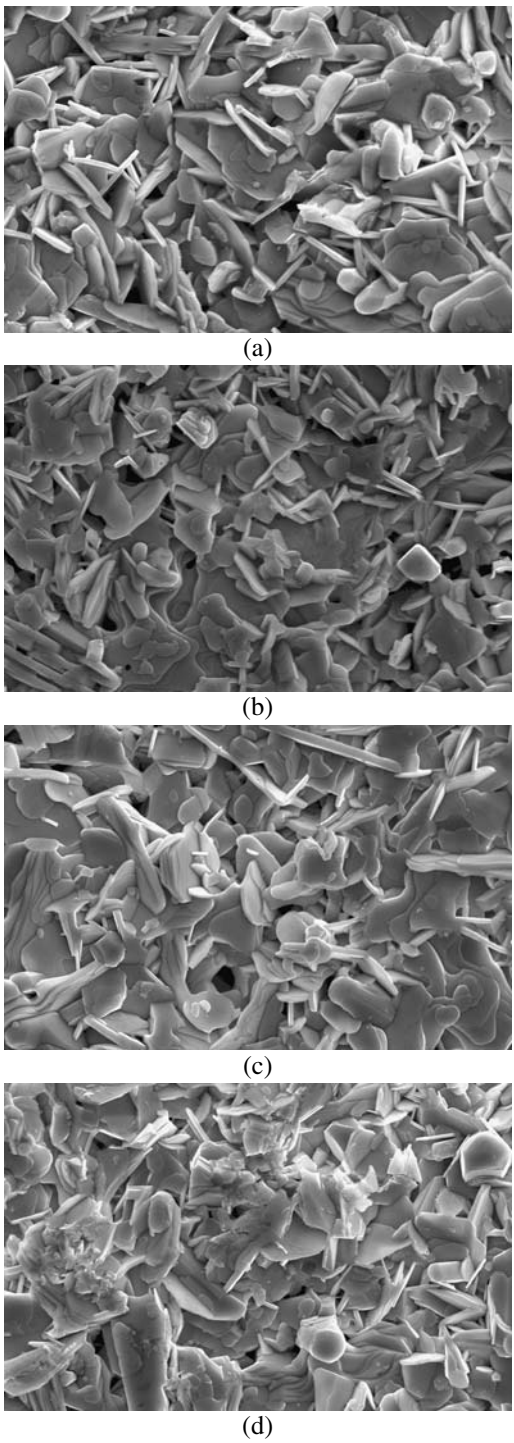

(a)

(b)

(c)

(d)

Fig. 2 SEM photograph of the samples A (**a**), B (**b**), C (**c**) and D (**d**) (20 kV, X2000, 10 μm)

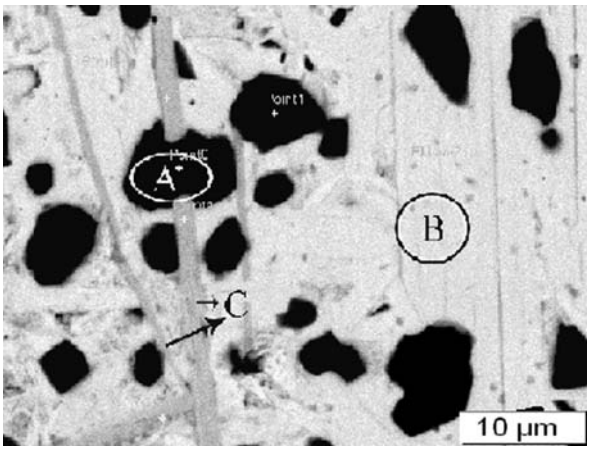

Fig. 3a SEM photograph of the polished surface of sample A. A denotes CuO rich phase, B denotes BiPb-2212 phase and C denotes BiPb-2223 phase

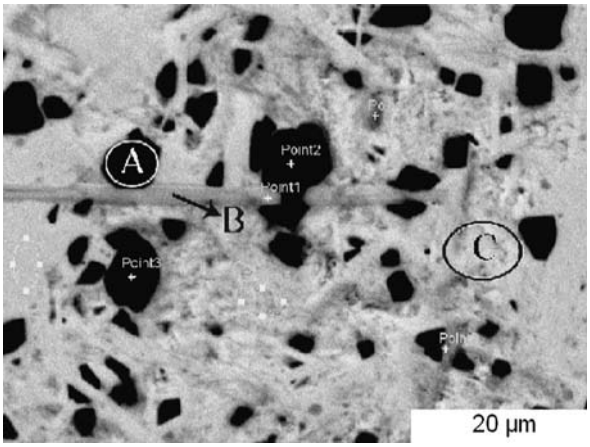

Fig. 3b SEM photograph of the polished surface of sample B. A denotes CuO rich phase, B denotes BiPb-2223 phase and C denotes BiPb-2212 phase

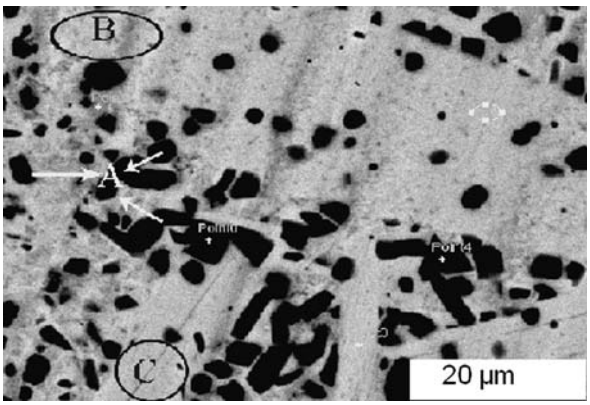

Fig. 3c SEM photograph of the polished surface of sample C. A denotes CuO rich phase, B denotes BiPb-2212 phase and C denotes BiPb-2223 phase

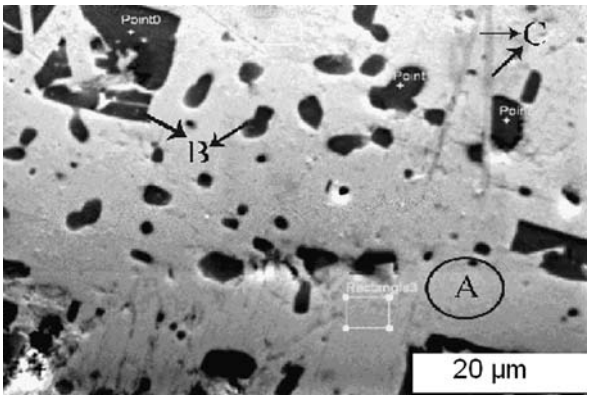

Fig. 3d SEM photograph of the polished surface of sample D. A denotes (2212) phase, B denotes Cu-rich impurity phase and C denotes BiPb-2223 phase

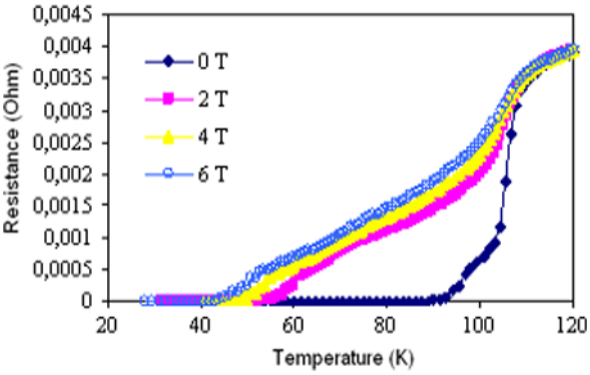

Fig. 4a (Color on-line) R versus T plots for the $Bi_{1.7}Pb_{0.3-x}Nd_xSr_2Ca_3Cu_4O_{12+y}$ system with $x = 0.025$ (sample A)

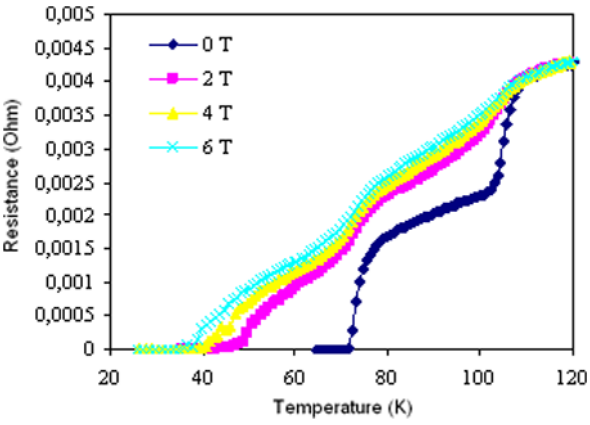

Fig. 4b (Color on-line) R versus T plots for the $Bi_{1.7}Pb_{0.3-x}Nd_xSr_2Ca_3Cu_4O_{12+y}$ system with $x = 0.050$ (sample B)

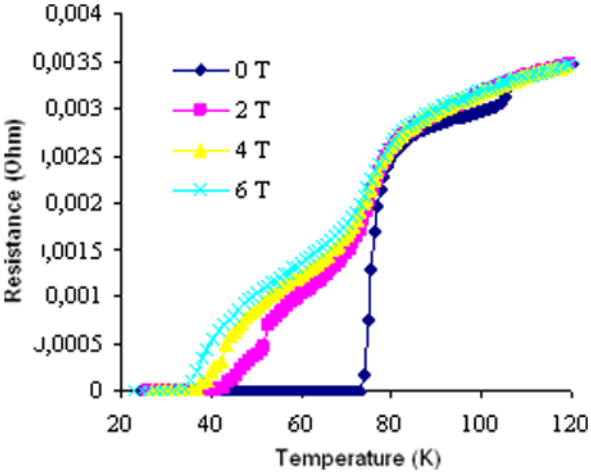

Fig. 4c (Color on-line) R versus T plots for the $Bi_{1.7}Pb_{0.3-x}Nd_xSr_2Ca_3Cu_4O_{12+y}$ system with $x = 0.075$ (sample C)

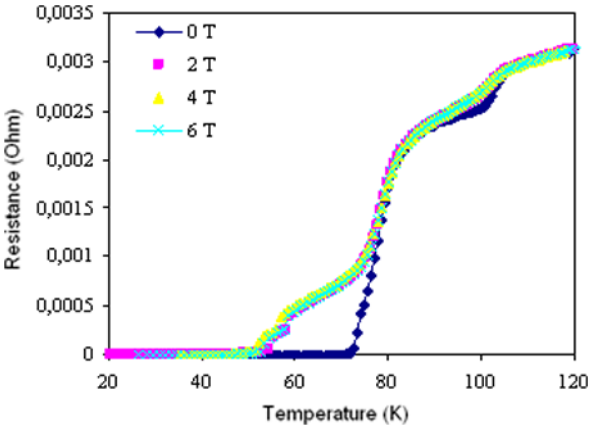

Fig. 4d (Color on-line) R versus T plots for the $Bi_{1.7}Pb_{0.3-x}Nd_xSr_2Ca_3Cu_4O_{12+y}$ system with $x = 0.1$ (sample D)

For the samples A, B, C and D, the $T_{c.onset}$'s were found to be 108.1, 107.8, 104.2 and 103.3 K, respectively and, $T_{c.offset}$'s were 92.8 for the sample A and 72 K for the samples B, C and D, in zero magnetic field. On the other hand, while the $T_{c.onset}$'s remained almost unchanged while $T_{c.offset}$'s decreased below 50 K by increasing the applied magnetic field.

These temperatures are comparable with the irreversibility or depinning temperatures [28]. It is well known that in type-II superconductors, electric field arises, electrical resistance and hence energy dissipation occurs when the driving Lorentz force per unit volume, $\mathbf{F}_L = \mathbf{J} \times \mathbf{B}$ exceeds the pinning force per unit volume $\mathbf{F}_P$. At lower temperature, a higher magnetic field is needed to depin the flux line since, lowering the temperature increases the pinning force. This results in a shift of the zero resistance temperature or the irreversibility temperature [21, 29, 30] downwards as the magnetic field increases.

We have displayed the graph of the normalized resistance (R/R_{110}) versus temperature T obtained between the onset and offset temperatures, in Fig. 5, for the

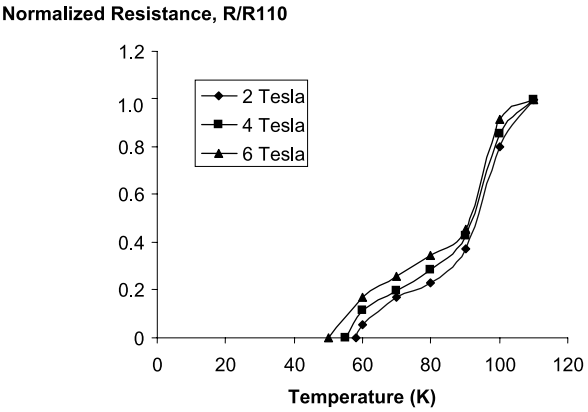

Fig. 5 Normalized resistance (R/R_{110}) against temperature for sample A in external magnetic fields of 2, 4 and 6 Tesla

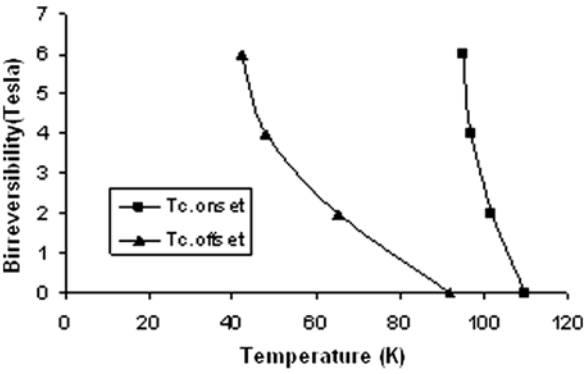

Fig. 6 Displays the comparison of the irreversibility lines for the $T_{c.onset}$ and $T_{c.offset}$ for sample A

sample A, in order to see the effect of applied magnetic field B_a on resistance. As can be seen from the figure, the resistances shift towards lower temperature values with increasing field. In Fig. 6, we have also presented the irreversibility magnetic field values, deduced from the resistances measurements, versus the onset and offset temperatures, for the sample A. It is obvious that while the variation of onset temperature is 15 K, the variation of offset temperature is about 50 K within the studied magnetic field range. It is generally proposed that the superconductivity is destroyed by increasing the rare-earth ions like Gd, Sm, Cd, Ce Nd, etc. in Bi superconducting system. The intergrowth of the impurity solid solution phases and formation of weak coupling between the impurity and superconducting grains also play a crucial role in diminishing the superconductivity. On the other hand, the optimum applied magnetic field can be hindered the negative effect arised from the impurities on the superconductivity. If the resistivity results revised, it can be seen that the $T_{c.offset}$ values start arising towards the high temperature values. So it can be concluded that the effects of the impurities are shielded by the magnetic field.

The number of holes, p, per Cu atom can be calculated by using the relation

$$\frac{T_c}{T_c^{max}} = 1 - 82.6(p - 0.16)^2$$

given by Presland et al. [31], where T_c^{max} is taken 110 K for the Bi-2223 system. Recently, this equation was successfully applied to the Bi-based superconducting systems [32–38]. Previous calculations for the unsubstituted Bi-2223 system have shown that the p-value ranged from 0.116 to 0.16. In this study, the p-values of the $x = 0.025, 0.050, 0.075$ and 0.1 samples have been calculated to be 0.174, 0.176, 0.185 and 0.187, respectively. The results obtained show that the p-values of our samples seem to increase slightly with increasing Nd concentration, however, are not much higher than the unsubstituted Bi-2223 system which points out that the amount of Nd dopant is far from the overdoped limit, in agreement with the results of Satyavathi et al. [21].

The magnetic hysteresis cycles (M–H) of the samples were performed at three different temperatures, 10, 20 and 30 K. Typical examples of magnetic hysteresis (M–H) loops of the samples A and D obtained are shown in Figs. 7 and 8. All of the samples prepared in this work have shown the similar behavior. We have found no anomalous magnetization behavior during the experiments. In all cases, the magnetization decreases with increasing temperature in agreement with the general characteristic of the high-T_c materials [11, 24]. All the samples exhibit weak field dependence particularly after 2 T and changes on the M–H curve rather small compared to the conventional superconducting materials.

The decrease of hysteresis loops with increasing temperature and the symmetrical behaviour of them imply existence of flux pinning centres. Thus might suggest that the magnetization behaviour at low fields is dominated by the bulk pinning rather than surface and geometrical barriers [50]. As can be seen from Figs. 7 and 8, due to the pinning effects and large volume of the superconducting regions, the field penetration becomes difficult below 10 K, but the applied fields begin to significantly penetrate into the samples at higher temperatures, due to the decrease of superconducting regions with increasing temperature. This is probably the reason for large decreases appearing in the breadth of magnetic hysteresis loops above 10 K.

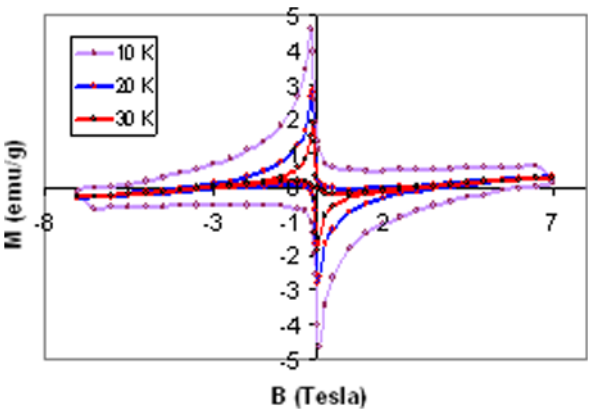

Fig. 7 M–H hysteresis of sample A

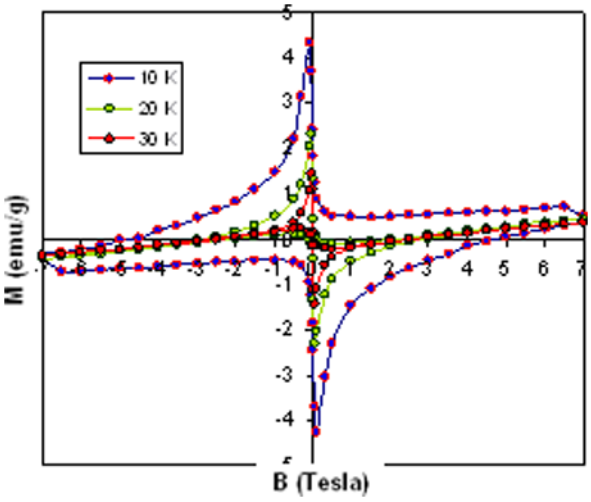

Fig. 8 (Color on-line) M–H hysteresis of sample D

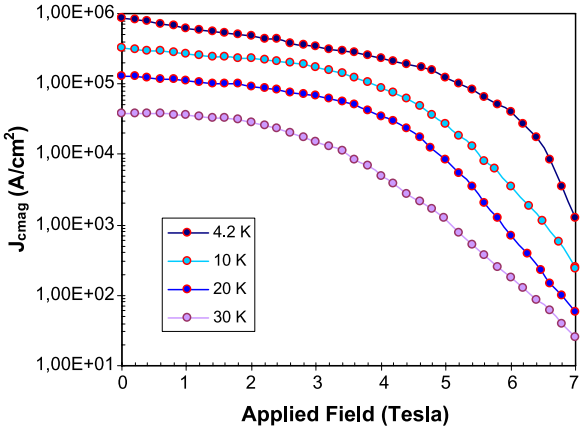

Fig. 9 J_{cmag} results of sample A

The $J_{\mathrm{c.mag}}$ values of the samples were determined using the Bean's model [39];

$$J_{\mathrm{c.mag}} = 20\frac{\Delta M}{a(1 - a/3b)}$$

where $J_{\mathrm{c.mag}}$ is the magnetization current density in amperes per square centimeter of a sample. $\Delta M = M_+ - M_-$ is measured in electromagnetic units per cubic centimeter, a and b ($a < b$) are the dimensions in centimeters of the cross-section of the sample parallel to the applied field. This model is used for calculation of J_{c} values in this study.

The calculated critical current densities of the samples as a function of the applied field, at a four different fixed temperatures are shown in Figs. 9 and 10. As can be seen from Fig. 9 and Table 2, the maximum value of $J_{\mathrm{c}}(8.51 \times 10^5$ A/cm$^2)$ is obtained at 4.2 K for optimally treated sample and then decreases with increasing temperature. All the samples prepared show that the field dependence of J_{cmag} is strong even at 4.2 K (Figs. 9 and 10). This kind of behavior can be explained in terms of weak grain

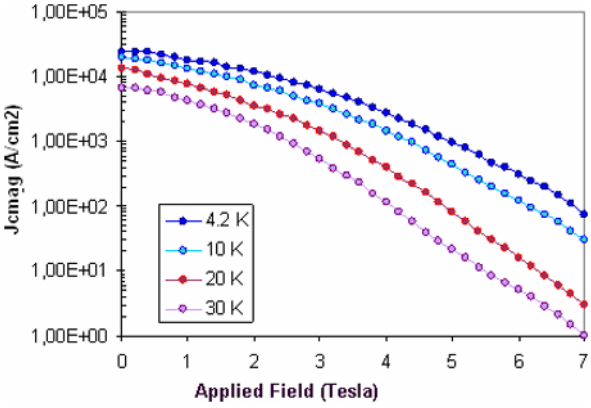

Fig. 10 (Color on-line) J_{cmag} result of sample D

Table 2 $J_{c.mag}$ result of samples A and D

Sample	J_{cmag} at 4.2 K A/cm^2	J_{cmag} at 10 K A/cm^2	J_{cmag} at 20 K A/cm^2	J_{cmag} at 30 K A/cm^2
A	8.51×10^5	3.3×10^5	1.28×10^5	3.8×10^4
D	2.43×10^5	1.94×10^5	1.28×10^4	6.6×10^3

connectivity and/or an increased volume fraction of impurity grains, such as CuO phase and formation of both BiPb-2212 and BiPb-2223 phases.

In general, higher values of J_c have been calculated while weak magnetic field dependence was still obtained at $T > 10$ K. This is expected because the magnetization curve of the sample forms a loop that indicates the presence of the pinning centers on the surface of the materials. It is also well known that in the high-T_c superconducting material, non-superconducting impurity phases are highly effective in the flux-pinning mechanism [47–49]. Thus, a higher critical current density with small amount of non-superconducting phases is possible.

Acknowledgements This work is supported by the Research Fund of Çukurova University, Adana, Turkey, under grant contracts no. AAP-2002-9, no. FBE.2004.D15.

References

1. P.W. Anderson, Science **235**, 1196 (1987)
2. P. Imbert, J.A. Hodges, J.B.M. da Cunha, Hyperfine Interact. **50**, 599 (1989)
3. M.A. Aksan, M.E. Yakıncı, Y. Balcı, J. Supercond. **15**, 553 (2002)
4. M.E. Yakıncı, J. Phys. Condens. Matter **9**, 1105 (1997)
5. M.A. Aksan, M.E. Yakıncı, Y. Balcı, Supercond. Sci. Technol. **13**, 955 (2000)
6. J. Jiang, J.J. Abell, Supercond. Sci. Technol. **11**, 7005 (1998)
7. J.P. Singh, J. Jou, N. Vasanthamahan, R.B. Poeppel, J. Matter Res. **8**, 2458 (1993)
8. B. Chevalier, B. Lepine, A. Lalerzin, J. Darriet, J. Eournau, J.M. Tarascon, Mater. Sci. Eng. 277 (1989)
9. B. Jayaram, P.C. Lanchester, M.T. Weller, Physica C **160**, 17 (1989)
10. M.M.A. Sekkina, H.A. El-Daly, K.M. Elsabawy, Supercond. Sci. Technol. **17**, 93 (2004)

11. A. Coşkun, A. Ekicibil, B. Özçelik, Chin. Phys. Lett. **19**(12), 1863 (2002)
12. J.M. Tarascon, P. Barboux, G.W. Hull, Phys. Rev. B **39**, 4316 (1989)
13. H. Yamanaka, H. Enomoto, J.S. Shin, Jpn. J. Appl. Phys. **30**, 645 (1991)
14. K.N. Kishore, M. Muralidhar, V.H. Babu, O. Pena, M. Sergent, F. Beniere, Physica C **204**, 299 (1993)
15. T. Kanai, T. Kamo, S. Matsuda, Jpn. J. Appl. Phys. **L551** 28 (1989)
16. M. Rateau, R. Suryanayarana, Physica (Utrecht) **162/164C**, 1199 (1989)
17. S. Simon, G. Ilonca, I. Barbur, Physica (Utrecht) **162/164C**, 1289 (1989)
18. H.J. Bornemann, D.E. Morris, H.B. Liu, P.K. Narwankar, Physica C **191**, 211 (1992)
19. C. Quitmann, D. Andrich, C. Jarchow, M. Fleuster, B. Beschoten, G. Guntherodt, Phys. Rev. B **46**, 11813 (1992)
20. P.N. Peters, R.C. Sisk, E.W. Urban, Appl. Phys. Lett. **52**, 2066 (1998)
21. S. Satyavathi, K.N. Kishore, V.H. Babu, O. Pena, Supercond. Sci. Technol. **9**, 93 (1996)
22. H.W. Zandbergen, W.A. Groen, A. Smit, G. Van Tendeloo, Physica C **168**, 426 (1990)
23. S. Satyavathi, M. Muralidhar, K.N. Kishore, V.H. Babu, O. Pena, M. Segent, F. Beriere, Appl. Supercond. **2**, 187–195 (1995)
24. A. Ekicibil, A. Coşkun, B. Özçelik, K. Kiymaç, Mod. Phys. Lett. B **19**, 331 (2005)
25. J.B. Mandal, S. Keshri, P. Mandal, A. Poddar, A.N. Das, B. Ghosh, Phys. Rev. B **46**, 11840 (1992)
26. F. Munakata, K. Matsuura, K. Kubo, T. Kawano, H. Yamauchi, Phys. Rev. B **45**, 10604 (1992)
27. K. Nanda Kishore, S. Satyavathi, M. Muralidhar, V.H. Babu, O. Pena, Phys. Status Solidi A **143**, 101 (1994)
28. Y. Xu, M. Seunega, Y. Gao, J.E. Crow, N.D. Spencer, Phys. Rev. B **42**, 8756 (1990)
29. Y. İye, T. Tamegai, H. Takeya, H. Takei, Jpn. J. Appl. Phys. Pt. 2 **26** L1057 (1987)
30. B. Oh, K. Char, A.D. Kent, M. Naito, M.R. Beasley, T.H. Geballe, R.H. Hammond, A. Kapitulnik, Phys. Rev. B **37**, 7861 (1998)
31. M.R. Presland, J.L. Tallon, R.G. Buckley, R.S. Liu, N.E. Floer, Physica C **176**, 95 (1991)
32. S.D. Obertelli, J.R. Cooper, J.L. Tallon, Phys. Rev. B **46**, 14928 (1992)
33. D.R. Sita, R. Singh, Physica C **296**, 21 (1998)
34. R. Wang, H. Sekine, H. Jin, Supercond. Sci. Technol. **9**, 529 (1996)
35. R. Singh, D.R. Sita, Physica C **312**, 289 (1999)
36. Z.W. Zhao, S.L. Li, H.H. Won, X.G. Li, Physica C **391**, 169 (2003)
37. M.A. Aksan, M.E. Yakıncı, J. Alloys Comp. **385**, 33 (2004)
38. Z. Özhanlı, M.E. Yakıncı, Y. Balcı, M.A. Aksan, J. Supercond. Incorp. Nov. Magn. **15**, 543 (2002)
39. C.P. Bean, Phys. Rev. Lett. **8**, 250 (1962)
40. S.M. Khalil, A. Sedky, Physica B **357**, 299–304 (2005)
41. S.M. Khalil, Phys. Status Solidi A **178**, 731 (2000)
42. M.M. Ibrahim, S.M. Khalil, A.M. Ahmed, J. Phys. Chem. Sol. **61**, 1553–1560 (2000)
43. M.M. Ibrahim, S.M. Khalil, EPJ Appl. Phys. **14**, 79–86 (2001)
44. D. Bahadur et al., Phys. Status Solidi A **123**, 591 (1991)
45. S.M. Khalil, A.M. Ahmed, Physica C **425**, 21–28 (2007)
46. M.A. Aksan, M.E. Yakıncı, Y. Balcı, Supercond. Sci. Technol. **13**, 955–963 (2000)
47. A. Ekicibil, A. Coşkun, B. Özçelik, K. Kıymaç, J. Low Temp. Phys. **140**, 105 (2005)
48. A. Ekicibil, A. Coşkun, B. Özçelik, K. Kıymaç, Mod. Phys. Lett. B **18**(23), 1–12 (2004)
49. A. Coşkun, A. Ekicibil, B. Özçelik, K. Kıymaç, Chin. J. Phys. **43**(2) (2005)
50. A. Coşkun, A. Ekicibil, B. Özçelik, K. Kıymaç, Chin. Phys. Lett. **21**(10), 2041 (2004)